


## Article

# Construction of ZnCdS Quantum-Dot-Modified CeO<sub>2</sub> (0D–2D) Heterojunction for Enhancing Photocatalytic CO<sub>2</sub> Reduction and Mechanism Insight

Junzhi Yan <sup>1</sup>, Yuming Sun <sup>1</sup>, Junxi Cai <sup>1</sup>, Ming Cai <sup>1</sup>, Bo Hu <sup>1</sup> , Yan Yan <sup>1,\*</sup>, Yue Zhang <sup>2,\*</sup> and Xu Tang <sup>1,\*</sup>

<sup>1</sup> School of Chemistry and Chemical Engineering, Institute for Advanced Materials, Jiangsu University, Zhenjiang 212013, China; yanjunzhi0923@163.com (J.Y.); s969678125@126.com (Y.S.); 18896660263@163.com (J.C.); cm1999@yeah.net (M.C.); hubo93@bcnu.edu.cn (B.H.)

<sup>2</sup> School of Chemistry and Chemical Engineering, Liaoning Normal University, Dalian 116029, China

\* Correspondence: dgy5212004@163.com (Y.Y.); zhangyue433@126.com (Y.Z.); tangxu@ujs.edu.cn (X.T.)

**Abstract:** It is important to improve the separation ability of photogenerated electrons and the adsorption capacity of carbon dioxide (CO<sub>2</sub>) for efficient photoreduction of CO<sub>2</sub>. Here, we synthesized ZnCdS quantum dots (ZCS-QDs) and cerium dioxide nanosheets (CeO<sub>2</sub>) using the solvothermal method and calcination method. We combined CeO<sub>2</sub> and ZCS-QDs to effectively enhance the charge separation efficiency, and the lifetime of photogenerated electrons was increased 4.5 times. The CO evolution rate of the optimized composite (ZCS-QDs/CeO<sub>2</sub>) was up to 495.8 μmol g<sup>-1</sup> h<sup>-1</sup>, and it had 100% product selectivity. In addition, the stability remained high after five cycles. The CO<sub>2</sub> adsorption capacity of the catalyst surface was observed by in situ FTIR. The test results showed that improving CO<sub>2</sub> capture ability and promoting photogenic electron separation had positive effects on enhancing photoreduction of CO<sub>2</sub>. This study provides a reference for constructing a zero-dimensional–two-dimensional (0D–2D) heterojunction and explores potential CO<sub>2</sub> reduction reaction mechanisms.

**Keywords:** photocatalysis; CO<sub>2</sub> reduction; CeO<sub>2</sub>; ZnCdS quantum dots



**Citation:** Yan, J.; Sun, Y.; Cai, J.; Cai, M.; Hu, B.; Yan, Y.; Zhang, Y.; Tang, X.

Construction of ZnCdS

Quantum-Dot-Modified CeO<sub>2</sub>

(0D–2D) Heterojunction for

Enhancing Photocatalytic CO<sub>2</sub>

Reduction and Mechanism Insight.

*Catalysts* **2024**, *14*, 599. [https://](https://doi.org/10.3390/catal14090599)

[doi.org/10.3390/catal14090599](https://doi.org/10.3390/catal14090599)

Academic Editor: Consuelo

Alvarez-Galvan

Received: 31 July 2024

Revised: 30 August 2024

Accepted: 4 September 2024

Published: 6 September 2024



**Copyright:** © 2024 by the authors. Licensee MDPI, Basel, Switzerland. This article is an open access article distributed under the terms and conditions of the Creative Commons Attribution (CC BY) license (<https://creativecommons.org/licenses/by/4.0/>).

## 1. Introduction

In recent years, the challenge of mitigating CO<sub>2</sub> emissions and converting this greenhouse gas into useful and renewable energy sources has been a focal point for contemporary research [1]. Photocatalysis is a promising strategy, particularly due to its potential for sustainability and relatively lower costs compared to other CO<sub>2</sub> reduction methods [2,3], and is widely used because of its low cost and sustainable advantages [4–6]. The steps of the photocatalytic CO<sub>2</sub> reduction reaction are complicated and affected by many factors, including light absorption, charge carrier generation, separation, and transfer, as well as surface reactions involving the adsorption and reduction of CO<sub>2</sub> [7]. In the field of photocatalysis, in order to improve the reaction rate and regulate the reaction pathway, researchers have made a lot of efforts [8], including reducing the particle size [9,10], loading metal onto the surface [11], dispersing to various carriers [12], etc. These methods improve the catalytic activity of the photocatalyst but only to a limited extent. Therefore, selecting a suitable photocatalyst to enhance the light absorption capacity and improve the photoelectron transport efficiency may be an effective means to improve the photocatalytic efficiency. Numerous studies have found that the selection of catalysts and system design plays a pivotal role in enhancing the overall efficiency of this process [13–15].

Two-dimensional (2D) cerium dioxide (CeO<sub>2</sub>) is a highly versatile material that has garnered significant interest in the realm of photocatalysis due to its excellent chemical and structural stability. In addition, the reversible switch between the Ce(III) and Ce(IV) states confers unique redox properties [16–18]. However, its wide bandgap typically

restricts its light absorption in the ultraviolet region, limiting its efficiency under visible light; this limitation hampers the direct conversion of CO<sub>2</sub> into fuels. Combining CeO<sub>2</sub> with other semiconductors to form CeO<sub>2</sub> heterojunctions (such as narrower-bandgap catalysts capable of absorbing visible light) seems to present an opportunity for strategic enhancement of light harvesting and charge separation efficiency. This approach leverages synergistic effects between the components, enhances light absorption, and promotes charge carrier dynamics.

The selection and engineering of catalysts that can not only effectively adsorb CO<sub>2</sub> but also facilitate efficient charge transfer are central to improving the photocatalytic conversion of CO<sub>2</sub> into renewable energy sources. Zero-dimensional (0D) quantum dot (QD) materials have been extensively investigated as the building blocks of photocatalysts due to their special quantum size effect, electron transfer properties, and their efficient absorption to visible light [19–21]. Ternary ZnCdS creates good conditions for adjusting the optical properties from the ultraviolet to the visible light range [22], and can adjust the appropriate bandgap range [23]. In fact, the use of QDs in combination with semiconductors in the field of photocatalysis has been reported in the past few years. For example, Yang et al. used Ag QDs anchored with CeO<sub>2</sub>, and the Ag QD/CeO<sub>2</sub> composite improved the utilization rate of visible light, and the photocatalytic elimination of acetaldehyde and water decomposition performance improved 7.08 and 6.83 times, respectively [24]. Jiang et al. reported a modification of CeO<sub>2</sub> using g-C<sub>3</sub>N<sub>4</sub> QDs, which improved the photoelectric response and showed significant performance improvement in the test of photoreduction of CO<sub>2</sub> [25]. Sre et al. deposited ZnCdS quantum dots on g-C<sub>3</sub>N<sub>4</sub> for photoinactivation of *E. coli* cells. The prepared composite photocatalyst enhanced the structural stability, as well as increased a large number of reaction sites, and improved the photocatalyst efficiency [26]. So, it can be inferred that if ZnCdS-QDs are introduced on the CeO<sub>2</sub> surface and they construct a 0D–2D heterojunction, the photocatalytic CO<sub>2</sub> activity and the recycling ability of the photocatalysts will be enhanced.

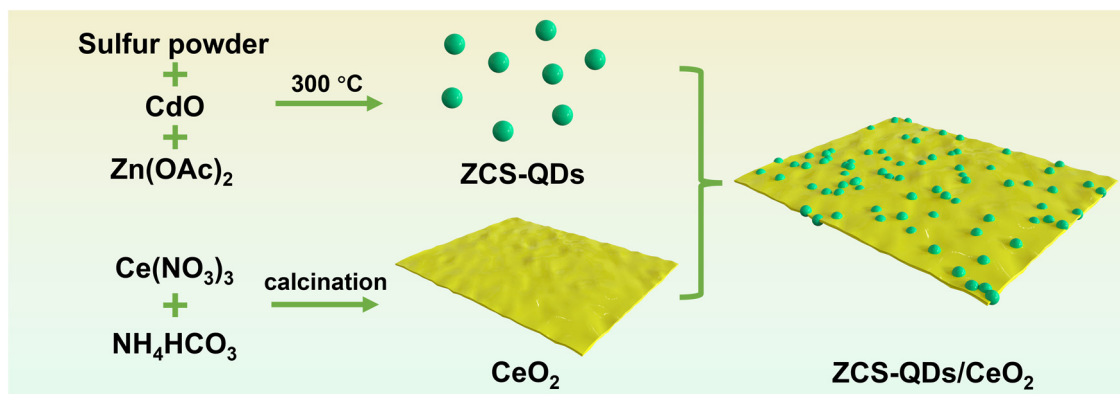
Inspired by the consideration above, ZnCdS quantum dots were combined with a CeO<sub>2</sub> heterojunction (ZCS-QDs/CeO<sub>2</sub>) and designed to optimize the energy band alignment and CO<sub>2</sub> reduction activity. The ZCS-QDs/CeO<sub>2</sub> exhibits a substantial increase in the lifetime of photogenerated electrons and achieves a remarkable CO evolution rate of 495.8 μmol g<sup>-1</sup> h<sup>-1</sup> without any sacrificial agents during the CO<sub>2</sub> reduction reaction, even showing good stability after five cycles. The in situ DRIFTS result provides direct evidence of the CO<sub>2</sub> adsorption dynamics on the CeO<sub>2</sub> surface and confirms the vital role of CeO<sub>2</sub> in enhancing substrate adsorption. Also, the observation of intermediates and monitoring changes in water and CO<sub>2</sub> consumption offer deeper insights into the photocatalytic process, contributing to a better understanding of the mechanism behind the improved efficiency.

## 2. Results and Discussion

### 2.1. Photocatalyst Characterization

Scheme 1 shows the synthesis strategy of ZCS-QDs/CeO<sub>2</sub>. Figure 1a shows the XRD patterns. For the CeO<sub>2</sub>, the four major diffraction peaks are located at 28.5°, 33.1°, 47.5°, and 56.3°, corresponding to the (111), (200), (220), and (311) lattice planes of CeO<sub>2</sub> (PDF#43-1002), respectively. For the ZCS-QDs, the six major diffraction peaks are located at 26.7°, 28.3°, 45.1°, 47.3°, 53.4°, and 56.2°, corresponding to the (002), (101), (102), (110), (103), and (200) lattice planes of ZnCdS (PDF#40-0834), respectively. The relatively small amount of ZCS-QDs and the partial coincidence of peak positions result in the ZCS-QDs' diffraction peak being covered by the CeO<sub>2</sub> diffraction peak; thus, no diffraction peak was observed for the ZCS-QDs in the ZCS-QDs/CeO<sub>2</sub> photocatalyst. The TEM image of CeO<sub>2</sub> is shown in Figure 1b, exhibiting a smooth two-dimensional sheet structure. The ZnCdS is uniformly dispersed and has a diameter of about 8 nm belonging to the morphology of the quantum dots (Figure 1c,d). From Figure 1e, it can be seen that quantum dots are fully grown on the 2D nanosheets, indicating that our catalyst of 0D–2D ZCS-QDs/CeO<sub>2</sub> is well assembled. Moreover, the 12% ZCS-QDs/CeO<sub>2</sub> was characterized by HRTEM. As shown in Figure 1f,

the measured lattice spacing of 0.33 nm and 0.31 nm corresponds to (002) of ZCS-QDs and (111) of CeO<sub>2</sub>, respectively. From HRTEM mapping (Figure 1g), the elements of S, Cd, Zn, O, and Ce were detected, providing further proof that the ZCS-QDs/CeO<sub>2</sub> has been successfully synthesized.



Scheme 1. Synthesis diagram of ZCS-QDs/CeO<sub>2</sub>.

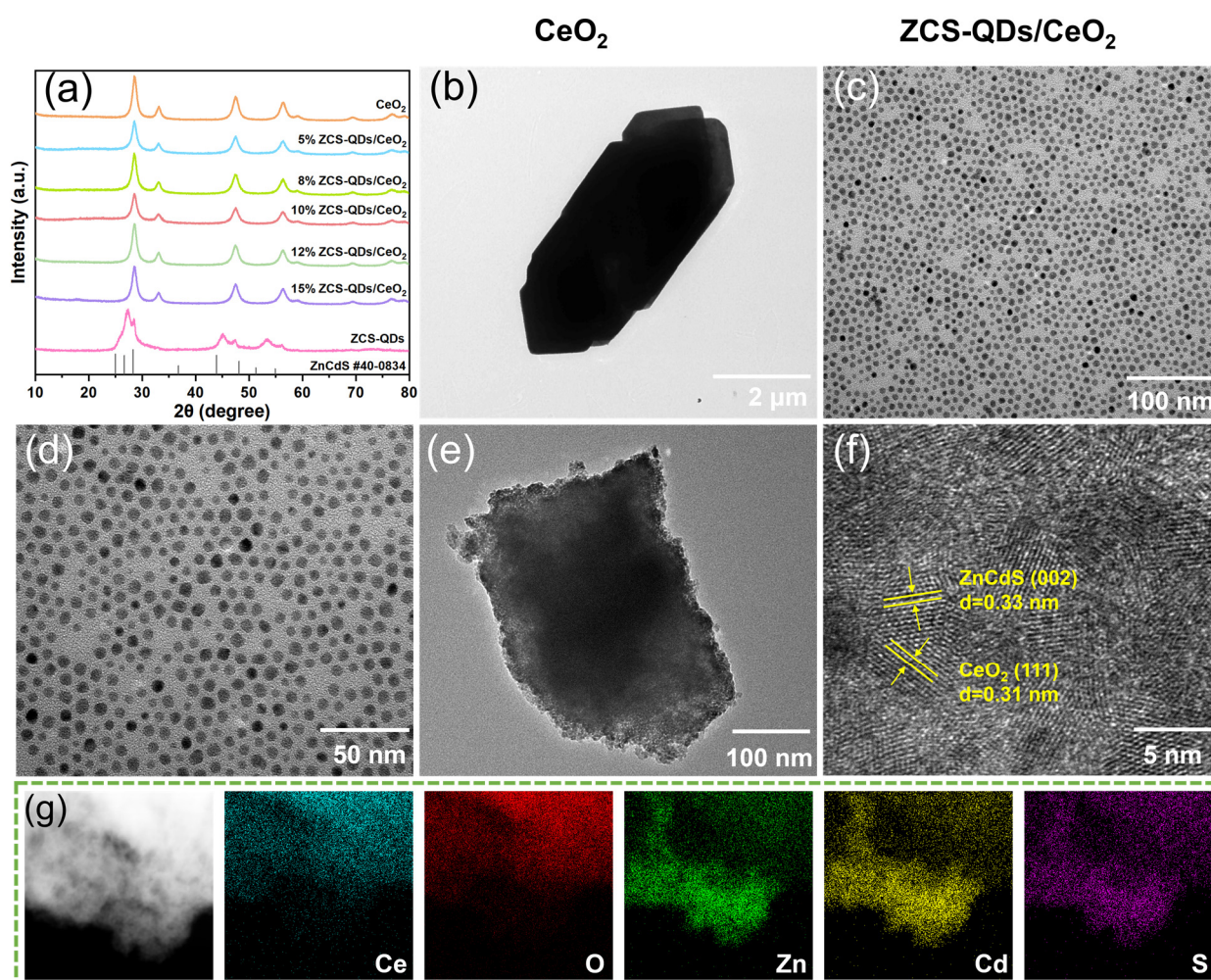
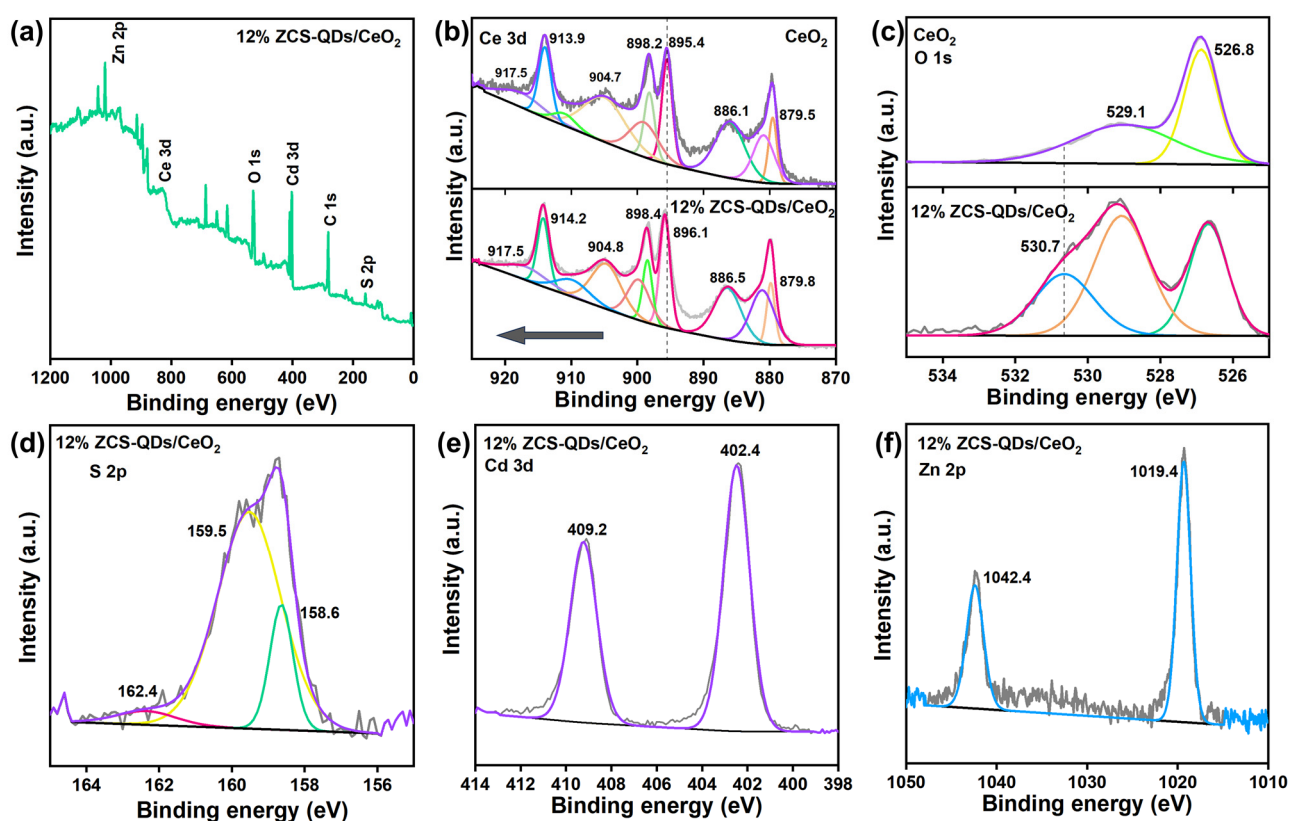


Figure 1. (a) XRD patterns of CeO<sub>2</sub>, ZCS-QDs, and x ZCS-QDs/CeO<sub>2</sub> (x = 5, 8, 10, 12, and 15%), (b–d) TEM image of CeO<sub>2</sub> and ZCS-QDs, (e) TEM image of 12% ZCS-QDs/CeO<sub>2</sub>, (f) HRTEM image of 12% ZCS-QDs/CeO<sub>2</sub>, (g) EDS elemental mapping images of 12% ZCS-QDs/CeO<sub>2</sub>.



## 2.2. Surface Composition and Photoelectric Analysis

The chemical state of the catalyst was investigated using X-ray photoelectron spectroscopy (XPS). From the XPS survey spectrum of Figure 2a, it can be seen that the Ce, O, S, Cd, and Zn elements are found in the 12% ZCS-QDs/CeO<sub>2</sub> catalyst. Figure 2b shows the Ce 3d levels for CeO<sub>2</sub> and 12% ZCS-QDs/CeO<sub>2</sub>. For CeO<sub>2</sub>, the peaks at 913.9 and 895.4 eV are from the Ce 3d<sup>9</sup> 4f<sup>0</sup> final state, and the peaks at 904.7, 898.2, 886.1, and 879.5 eV are from the Ce 3d<sup>9</sup> 4f<sup>2</sup> and Ce 3d<sup>9</sup> 4f<sup>1</sup> final states [27]. However, for 12% ZCS-QDs/CeO<sub>2</sub>, the peak position of 895.4 eV shifted to 896.1 eV. This was attributed to the interaction of ZCS QDs and CeO<sub>2</sub>, and resulted in the electron transfer in ZCS-QDs/CeO<sub>2</sub>. For the O 1s of CeO<sub>2</sub> (Figure 2c), two characteristic peaks can be observed at 529.1 and 526.8 eV, representing lattice oxygen and adsorbed oxygen, respectively [28], in the spectrum of 12% ZCS-QDs/CeO<sub>2</sub>. When CeO<sub>2</sub> is combined with the nanostructure, the surface oxygen site will greatly affect the reduction reaction of the semiconductor at the interface [29]. In addition, oxygen sites are often involved in constructing the support interface for reactivity, as well as the reaction site of various adsorbents on the carrier [30,31]. Therefore, the new characteristic peak at 530.7 eV is attributed to S-O [32]. For the S 2p spectrum of 12% ZCS-QDs/CeO<sub>2</sub> (Figure 2d), 159.5 and 158.6 eV are attributed to S 2p<sup>1/2</sup> and S 2p<sup>3/2</sup> [33], respectively, while the characteristic peak at 162.4 eV was attributed to the newly formed S-O. The formation of S-O fully confirms that a close chemical interaction is formed between ZCS-QDs and CeO<sub>2</sub>, which provides good conditions for electron transfer during the reaction. Two characteristic peaks at 409.2 and 402.4 eV can be observed in the Cd 3d spectrum (Figure 2e), corresponding to Cd 3d<sup>3/2</sup> and Cd 3d<sup>5/2</sup>, respectively [33]. Two characteristic peaks can be observed at 1042.4 and 1019.4 eV in the Zn 2p spectrum (Figure 2f), corresponding to Zn 2p<sup>1/2</sup> and Zn 2p<sup>3/2</sup> [34], respectively.



**Figure 2.** XPS spectra of (a) survey spectra, (b) Ce 3d, (c) O 1s, (d) S 2p of 12% ZCS-QDs/CeO<sub>2</sub>, (e) Cd 3d of 12% ZCS-QDs/CeO<sub>2</sub>, and (f) Zn 2p of 12% ZCS-QDs/CeO<sub>2</sub>.

The light absorption capacity of the photocatalyst was measured by UV–Vis DRS [35] (Figure 3a). The CeO<sub>2</sub> showed strong absorption properties in the ultraviolet region and an absorption range of ZCS-QDs located at 480 nm. However, 12% ZCS-QDs/CeO<sub>2</sub> has a unique enhanced adsorption peak around 450–620 nm. Also, the bandgap value was calculated and showed in Figure 3b using the following formula:

$$(\alpha h\nu)^{1/n} = A(h\nu - E_g)$$

where  $\alpha$ ,  $h\nu$ ,  $E_g$ , and  $A$  represent the absorption coefficient, photon energy, bandgap energy, and proportionality constant, respectively. ZCS-QDs/CeO<sub>2</sub> has the narrowest bandgap of 2.61 eV, and the bandgaps of ZCS-QDs and CeO<sub>2</sub> were 2.67 eV and 2.98 eV. In addition, the valence band (VB) positions of CeO<sub>2</sub> and ZCS-QDs were determined by VB-XPS (Figure 3c,d); the corresponding VBs are 1.45 eV and 2.38 eV. Based on the above results, the band structures of CeO<sub>2</sub> and ZCS-QDs were obtained, as shown in Figure 3e.

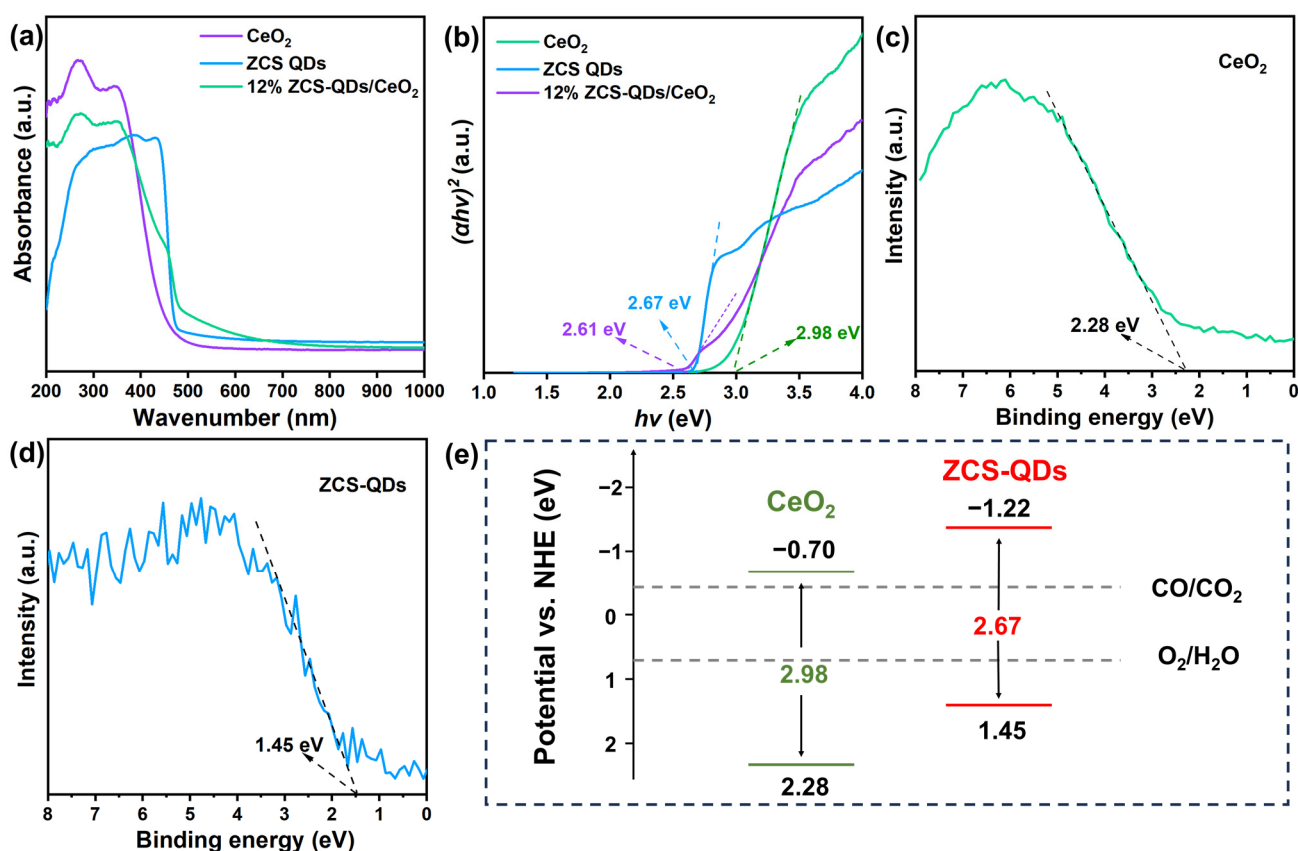


**Figure 3.** (a) UV–Vis DRS, (b) plots of  $(\alpha h\nu)^{1/2}$  versus  $(h\nu)$ , (c,d) VB-XPS spectra of CeO<sub>2</sub> and ZCS-QDs, and (e) bandgap structure diagram of CeO<sub>2</sub> and ZCS-QDs.

Figure 4a shows the results of TR-PL spectroscopy. The lifetimes of CeO<sub>2</sub> and ZCS-QDs are 2.53 ns and 6.67 ns, and 12% ZCS-QDs/CeO<sub>2</sub> has the longest average decay life with 30.17 ns, meaning that 12% ZCS-QDs/CeO<sub>2</sub> has excellent charge separation ability. As shown in Figure 4b, transient photocurrent responses (TPRs) were recorded, and all the catalysts exhibited stable photocurrent densities. It is worth noting that 12% ZCS-QDs/CeO<sub>2</sub> has the highest photocurrent density compared to CeO<sub>2</sub> and ZCS-QDs. Also, 12% ZCS-QDs/CeO<sub>2</sub> has the smallest EIS radius (Figure 4c). This means that 12% ZCS-QDs/CeO<sub>2</sub> has the smallest charge transfer resistance. The above confirmed that 12% ZCS-QDs/CeO<sub>2</sub> has the best charge transfer ability and shows the best photocatalytic ability.

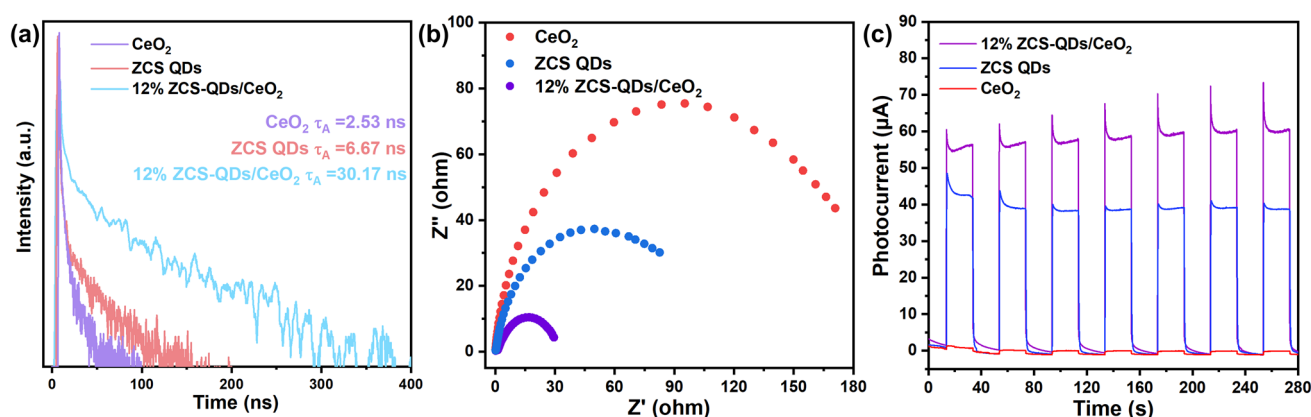


**Figure 4.** (a) TR-PL decay spectra of  $\text{CeO}_2$ , ZCS-QDs, and  $12\% \text{ ZCS-QDs/CeO}_2$ ; (b) TPR and (c) EIS of  $\text{CeO}_2$ , ZCS-QDs, and  $12\% \text{ ZCS-QDs/CeO}_2$ .

### 2.3. Photocatalytic Activity

As shown in Figure 5a, the  $\text{CO}_2$  photoreduction activity of  $\text{CeO}_2$ , ZCS-QDs, and  $x\text{-ZCS-QDs/CeO}_2$  ( $x$  means the different amount of ZCS-QDs) was determined. The  $\text{CO}$  yield of ZCS-QDs is  $151.8 \mu\text{mol g}^{-1} \text{h}^{-1}$ . For the  $x \text{ ZCS-QDs/CeO}_2$ , the  $\text{CO}_2$  reduction performance significantly increased with all values of  $x$ , and  $12\% \text{ ZCS-QDs/CeO}_2$  achieved the highest performance ( $495.8 \mu\text{mol g}^{-1} \text{h}^{-1}$ ), increasing 3.3 times. However, the  $\text{CO}_2$  reduction activity of  $15\% \text{ ZCS-QDs/CeO}_2$  decreased because the excessive number of ZCS-QDs cover the  $\text{CO}_2$  adsorption sites on the  $\text{CeO}_2$  surface and inhibit  $\text{CO}_2$  adsorption. In order to exclude the effect of decomposition of organic matter from the catalyst, a controlled experiment under  $\text{N}_2$  was conducted. No  $\text{CO}$  was detected (Figure 5b), which confirmed that all of the  $\text{CO}$  product comes from  $\text{CO}_2$  conversion. To investigate the stability of  $12\% \text{ ZCS-QDs/CeO}_2$ , cyclic experiments were conducted. It can be seen from Figure 5c that, after five cycles, the  $12\% \text{ ZCS-QDs/CeO}_2$  still had high catalytic activity, meaning that the catalyst has good stability. This study was compared with values previously reported for  $\text{CeO}_2$ -based materials, such as  $\text{CeO}_2/\text{TiO}_2$  ( $\text{CO}$  yield of  $61.9 \mu\text{mol g}^{-1} \text{h}^{-1}$ ) [36],  $\text{CuO-CeO}_2/\text{TiO}_2$  NT ( $\text{CO}$  yield of  $9.2 \mu\text{mol g}^{-1} \text{h}^{-1}$ ) [37],  $\text{CeO}_2/\text{g-C}_3\text{N}_4$  ( $\text{CO}$  yield of  $31 \mu\text{mol g}^{-1} \text{h}^{-1}$ ) [38], and  $\text{CoAl-LDH/CeO}_2/\text{RGO}$  ( $\text{CO}$  yield of  $5.5 \mu\text{mol g}^{-1} \text{h}^{-1}$ ) [39]. Among many  $\text{CeO}_2$ -based photocatalysts, ZCS-QDs have the highest  $\text{CO}$  evolution rate. It is fully confirmed that ZCS-QDs/ $\text{CeO}_2$  has great advantages in the field of efficient photocatalytic reduction of  $\text{CO}_2$ .

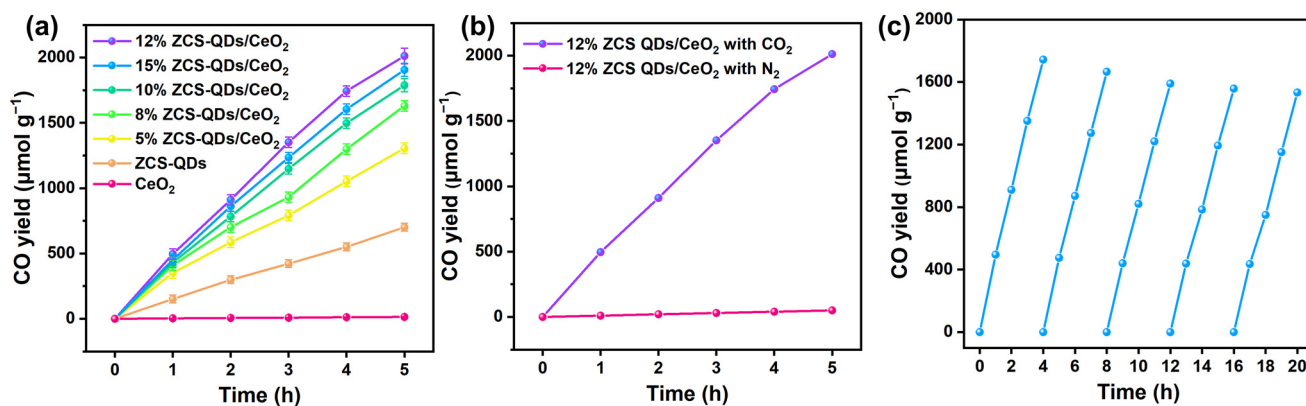


**Figure 5.** (a) Photocatalytic activity of  $\text{CeO}_2$ , ZCS-QDs, and  $x \text{ ZCS-QDs/CeO}_2$ ; (b) photocatalytic performance of  $12\% \text{ ZCS-QDs/CeO}_2$  under  $\text{CO}_2$  and  $\text{N}_2$ ; (c) cycling test of  $12\% \text{ ZCS-QDs/CeO}_2$ .

#### 2.4. Mechanism of CO<sub>2</sub> Photoreduction

It is known that the CO<sub>2</sub> adsorption capacity of catalysts is crucial for the photocatalytic reduction reaction. Thus, CO<sub>2</sub> adsorption tests were performed by in situ DRIFTS. As shown in Figure 6a,b, the adsorption capacity of CeO<sub>2</sub> for CO<sub>2</sub> is significantly higher than that of ZCS-QDs (the peak at 2340 cm<sup>-1</sup> is a characteristic peak of CO<sub>2</sub>), indicating that CeO<sub>2</sub> has strong CO<sub>2</sub> adsorption capacity. However, due to the wide bandgap of CeO<sub>2</sub> and the fact that it has fewer active sites, it is difficult to effectively convert the surface-adsorbed CO<sub>2</sub> into CO, CH<sub>4</sub>, and other high value-added products. Although, the CO<sub>2</sub> adsorption strength of 12% ZCS-QDs/CeO<sub>2</sub> decreased slightly compared with that of CeO<sub>2</sub>, it was still higher than that of ZCS-QDs (Figure 6c). The weakened CO<sub>2</sub> adsorption could be caused by the ZCS-QDs covering some of the adsorption sites of CeO<sub>2</sub>.

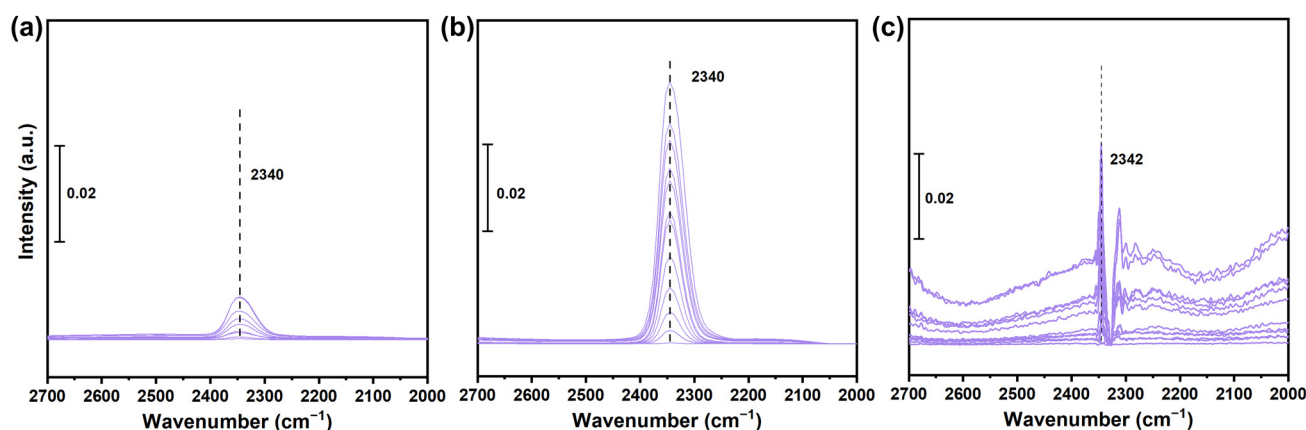


**Figure 6.** DRIFTS spectra of CO<sub>2</sub> adsorption of (a) ZCS-QDs, (b) CeO<sub>2</sub>, and (c) 12% ZCS-QDs/CeO<sub>2</sub>.

In order to investigate the photoreduction CO<sub>2</sub> mechanism, in situ DRIFTS was carried out. Using the pre-reaction equilibrium state as a blank background, positive or negative infrared signals during the reaction were used to represent the increase or disappearance of substances on the interface. Figure 7a,b represent the CO<sub>2</sub> photoreduction processes of CeO<sub>2</sub> and ZCS-QDs. The peaks at 2339 cm<sup>-1</sup> and 1658 cm<sup>-1</sup> correspond to CO<sub>2</sub> and H<sub>2</sub>O consumption signals, respectively [40]. By comparing the signal strength, the  $A_{2339}/A_{1658}$  of CeO<sub>2</sub> is 0.27, and the  $A_{2339}/A_{1658}$  of ZCS-QDs is 0.31. In 12% ZCS-QDs/CeO<sub>2</sub> (Figure 7c),  $A_{2344}/A_{1668}$  is 2.08; this result suggests that CeO<sub>2</sub> and ZCS-QDs mainly consume H<sub>2</sub>O during the photoreaction, while 12% ZCS-QDs/CeO<sub>2</sub> consumes CO<sub>2</sub> and converts it into CO. The above results show that after CeO<sub>2</sub> captures CO<sub>2</sub>, photogenerated electrons migrate to the catalyst surface and react with CO<sub>2</sub>, greatly inhibiting competitive reactions of H<sub>2</sub>O splitting. Moreover, in Figure 7c, during 12% ZCS-QDs/CeO<sub>2</sub> photoreaction, a series of peaks can be observed. The positive signal peak appearing at 2355 cm<sup>-1</sup> is the protonated CO<sub>2</sub> intermediate (O=C=O-H<sup>+</sup>) [41]. The peaks at 1468 cm<sup>-1</sup> correspond to COOH\* species [42]. In addition, the peak at 1402 cm<sup>-1</sup> corresponds to carbonate (m-CO<sub>3</sub><sup>2-</sup>), the peak at 1267 cm<sup>-1</sup> belongs to bidentate carbonate (b-CO<sub>3</sub><sup>2-</sup>), and the peak at 1145 cm<sup>-1</sup> represents bicarbonate (HCO<sub>3</sub><sup>-</sup>) [43–45].

Based on the discussion of the above results, the 0D–2D ZCS-QDs/CeO<sub>2</sub> heterojunction is used for selective photoreduction of CO<sub>2</sub> to CO. Under visible light (300 W xenon lamp) irradiation, both CeO<sub>2</sub> and ZCS-QDs can absorb ultraviolet light and part of the visible light spectrum to produce electrons and holes [46–48]. As CeO<sub>2</sub> and ZCS-QDs have a CB position of -0.7 eV and -1.22 eV, they both have the potential for CO<sub>2</sub> reduction of CO. When the two materials were combined together, a Z-heterojunction was formed. The electrons on the CB of CeO<sub>2</sub> recombine with the holes from the VB of ZCS-QDs; this not only improves the efficiency of photogenerated carrier separation but also the high-reducing-capacity photogenerated electrons on ZCS-QDs react with CO<sub>2</sub> and further

improve the efficiency of photoreduction of CO<sub>2</sub> to CO (Figure 8). The CO<sub>2</sub> photoreduction process over ZCS-QDs/CeO<sub>2</sub> can be inferred as follows:

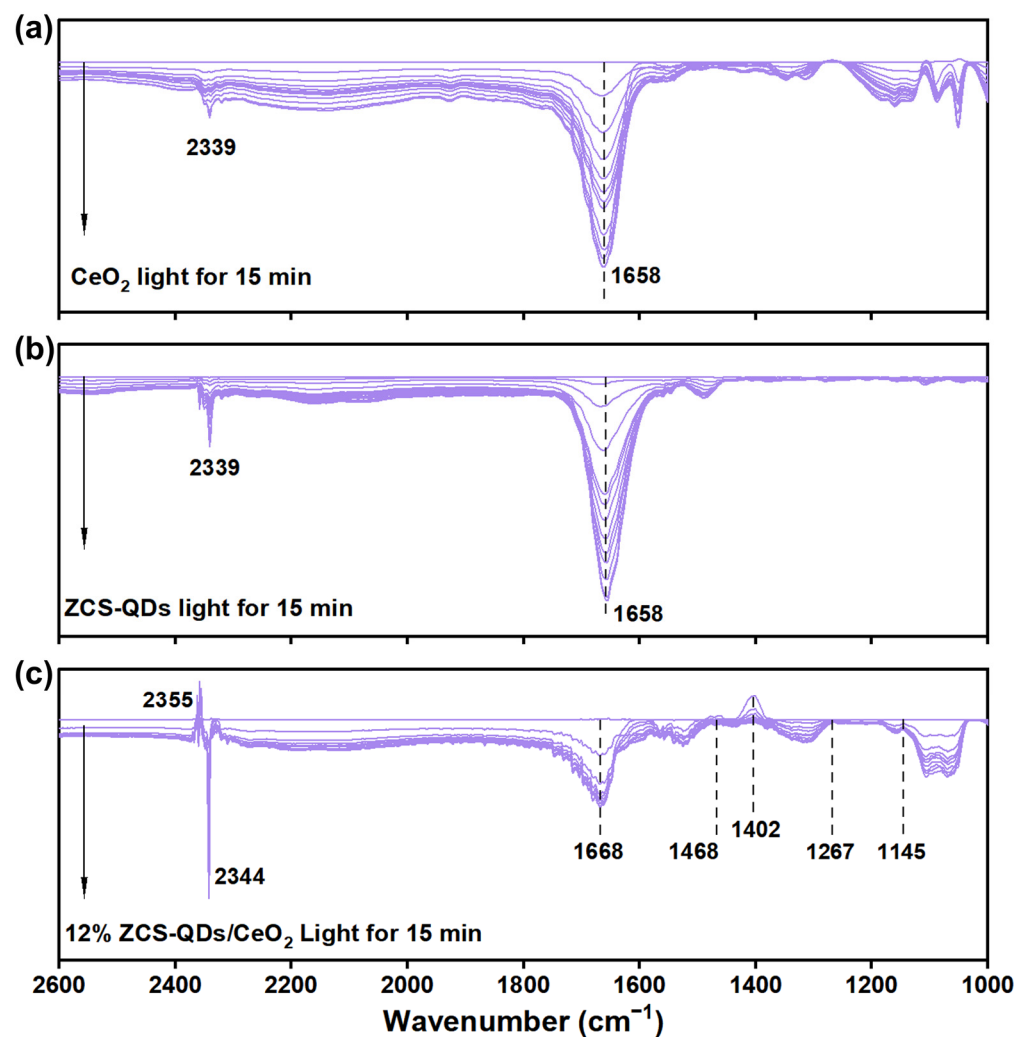
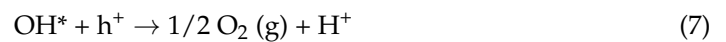
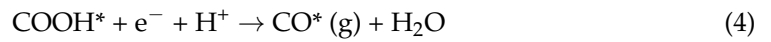
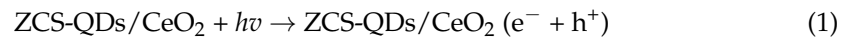
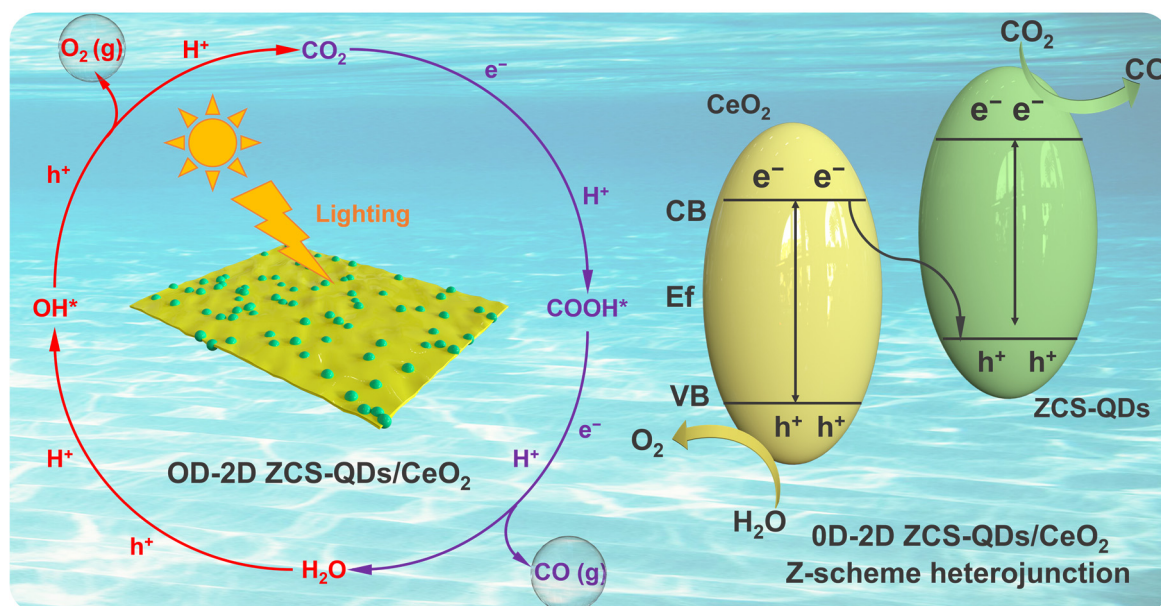


Figure 7. DRIFTS spectra of (a) CeO<sub>2</sub>, (b) ZCS-QDs, and (c) 12% ZCS-QDs/CeO<sub>2</sub>.





**Figure 8.** Photocatalytic CO<sub>2</sub> reduction mechanism of 0D–2D ZCS-QDs/CeO<sub>2</sub>.

### 3. Experimental Section

#### 3.1. Methods

##### 3.1.1. Materials

Sulfur powder (99.999%), 1-octadecene (ODE, 90%), oleic acid (OA, 90%), cadmium oxide (CdO, 99.99%), zinc acetate (Zn(OAc)<sub>2</sub>, 99.99%), 11-mercaptopundecanoic acid (MUA, 95%), n-hexane (97%) tetramethylammonium hydroxide pentahydrate (97%), cerium nitrate hexahydrate (Ce(NO<sub>3</sub>)<sub>3</sub>·6H<sub>2</sub>O, 99.5%), ammonium bicarbonate (NH<sub>4</sub>HCO<sub>3</sub>, 99.995%), acetone (99.5%), methyl alcohol (99.5%), and ethyl alcohol (99.7%) were purchased from Sinopharm Chemical Reagent Co., Ltd. (Shanghai, China).

##### 3.1.2. Synthesis of ZCS-QDs

The ZCS-QD synthesis method was improved according to the reported procedure [49]. For the S-precursor, 0.51 g of sulfur powder was dissolved in 16 mL of ODE and heated to 150 °C under N<sub>2</sub>. For the ZnCd-precursor, 0.256 g of CdO and 0.368 g of Zn(OAc)<sub>2</sub> were dissolved in a mixture of 13 mL of ODE and 6 mL of OA and then heated to 300 °C under N<sub>2</sub>.

A total of 4 mL of S-precursor was injected into the ZnCd-precursor and held at 300 °C for 10 min. When brought to room temperature, the quantum dots were precipitated with acetone and then dispersed in n-hexane for preservation.

##### 3.1.3. Ligand Exchange of ZCS-QDs

For ligand exchange, we used methods that have been previously reported [50]. A total of 20 mg of MUA was dissolved into 15 mL of methanol and the pH of the solution was adjusted to >10 using tetramethylammonium hydroxide pentahydrate. Then, 20 mg worth of ZCS-QDs was added to the above mixed solution, and stirred overnight at 60 °C in a N<sub>2</sub> atmosphere. The QDs were precipitated with ethyl acetate, then cleaned with acetone and dispersed in water for preservation.

##### 3.1.4. Synthesis of CeO<sub>2</sub>

For solution A, 2.78 g of Ce(NO<sub>3</sub>)<sub>3</sub>·6H<sub>2</sub>O was added to 100 mL of water and stirred for 30 min. For solution B, 1.50 g of NH<sub>4</sub>HCO<sub>3</sub> was added to 100 mL of water and stirred for 30 min. The two solutions, A and B, were mixed and stirred for 1h, left stationary at

30 °C for 24 h, and then centrifugally dried. Last calcination was performed at 500 °C for 4 h in an air atmosphere.

### 3.1.5. Synthesis of x ZCS-QDs/CeO<sub>2</sub>

A certain amount of CeO<sub>2</sub> was added to ZCS-QD solutions of different volumes, stirred away from light for 24 h, and centrifugally dried to obtain x ZCS-QDs/CeO<sub>2</sub>.

## 3.2. Characterizations

Transmission electron microscopy (TEM) analyses were performed on an H-7800 microscope (Hitachi, Tokyo, Japan) with an acceleration voltage of 120 kV. High-resolution transmission electron microscopy (HRTEM) was carried out on a JEM-2010 transmission electron microscope (Tokyo, Japan). The XRD patterns were examined on a Shimadzu-6100 powder X-ray diffractometer (Tokyo, Japan) using Cu K $\alpha$  radiation at a scan rate of 10° min<sup>-1</sup>. Transient fluorescence spectra were produced on an Edinburgh FLS1000 (Edinburgh, UK). The surface chemical states of the samples were studied by X-ray photoelectron spectroscopy (XPS, Thermo Scientific K-Alpha, Waltham, MA, USA). The optical properties of the photocatalyst were studied using UV-Vis diffuse reflectance spectroscopy (DRS, UV-2450 Shimadzu, Kyoto, Japan). Time-resolved photoluminescence (TRPL, Edinburgh FLS1000, UK) attenuation curves were obtained using a photoluminescence detector. In situ diffuse reflection infrared Fourier transform spectroscopy (DRIFTS) experiments were conducted on a Nicolet iS10 (Thermo) machine. In a typical procedure, the catalyst sample was sealed in a reaction chamber with a quartz window. CO<sub>2</sub> and H<sub>2</sub>O were carried into the reaction chamber by N<sub>2</sub> flow until equilibrium. Taking the equilibrium system before reaction as the blank background, IR signals were collected in situ during the incident irradiation of a 365 nm LED lamp (3W, Education Au-light Co., Ltd., Beijing, China) through the quartz glass window. In the in situ CO<sub>2</sub> adsorption experiment, CO<sub>2</sub> with progressively increasing concentration was introduced into the chamber and infrared signals were collected until the adsorption equilibrium was reached.

### 3.3. CO<sub>2</sub> Photoreduction Experiments

CO<sub>2</sub> photoreduction was carried out in a sealed 150 mL quartz reactor with a 300 W Xenon lamp (1000 mW cm<sup>-2</sup>, Education Au-light Co., Ltd., Beijing, China) as the white light source. In a typical procedure, 10 mg of catalyst was dispersed in 3 mL of deionized water. The resulting mixture was dropped on quartz glass and then dried at 60 °C. The dried catalyst was placed in the quartz reactor with 1 mL of H<sub>2</sub>O. CO<sub>2</sub> was then introduced into the reactor for 30 min to completely remove the air. During the reaction, a Xenon lamp illuminated the catalyst sample through the quartz window (22.1 cm<sup>2</sup>). Gas products were detected by a gas chromatograph (GC-7920, Beijing, China) equipped with a hydrogen flame ionization detector (FID).

### 3.4. Photoelectrochemical Measurements

The photoelectric chemistry experiment was tested on the electrochemistry workstation (CHI 660E, Shanghai Chenhua Instrument Co., Ltd., Shanghai, China). The reaction was carried out in a homemade standard three-electrode cell. The reference electrode and the reverse electrode were saturated Ag/AgCl and Pt electrodes, respectively, and 0.5 M Na<sub>2</sub>SO<sub>4</sub> solution was used as the electrolyte. The 0.02 g photocatalyst, 0.03 mL oleic acid, 0.01 g PVP were dispersed into 3 mL ethanol and ultrasonic for 1 h. The prepared suspension is then uniformly dropped onto the FTO glass. Using 300 W xenon lamp as light source, the effective area is about 1 cm<sup>2</sup>.

## 4. Conclusions

In summary, the 0D–2D ZCS-QDs/CeO<sub>2</sub> heterojunction was successfully prepared using solvothermal and calcination methods, and it was used in a high-efficiency photocatalytic CO<sub>2</sub> reduction reaction. When using no sacrificial agent, the CO evolution rate

reached  $495.8 \mu\text{mol g}^{-1} \text{h}^{-1}$ , which was 3.3 times higher than that of the ZCS-QD monomer, and has 100% selectivity. After five cycles, the catalytic activity was still high. This efficient photoconversion of  $\text{CO}_2$  can be attributed to the combination of two monomers, ZCS-QDs and  $\text{CeO}_2$ , which promote the effective separation of photogenerated electrons, and the lifetime of photogenerated electrons is increased by 4.5 times. In addition, in situ FTIR was used to observe the changes in  $\text{H}_2\text{O}$  and  $\text{CO}_2$  consumption during the reaction and monitor the formation of intermediate products. The result shows that the adsorption of  $\text{CO}_2$  on the surface of  $\text{CeO}_2$  solves the problem of low porosity on the surface of ZCS-QDs, creating good conditions for efficient photoreduction of  $\text{CO}_2$ . The formation of intermediates such as  $\text{COOH}^*$ ,  $\text{m-CO}_3^{2-}$ ,  $\text{b-CO}_3^{2-}$ ,  $\text{HCO}_3^-$ , and  $\text{OH}^*$  was monitored. Therefore, a well-designed ZCS-QDs/ $\text{CeO}_2$  heterojunction can be used as an effective composite photocatalyst. In the future design of photocatalysts, synergistically improving both the  $\text{CO}_2$  capture ability and the photoelectron separation efficiency is an effective means to improve the efficiency of the photocatalyst. This provides a new strategy for efficient  $\text{CO}_2$  conversion.

**Author Contributions:** Investigation, data curation, and writing of the original draft, J.Y. and X.T.; resources, Y.S. and J.C.; writing—review, M.C., B.H. and Y.Z.; conceptualization, supervision, and writing—review and editing, Y.Y. All authors have read and agreed to the published version of the manuscript.

**Funding:** This research was funded by the National Natural Science Foundation of China (No. 22208127), the Senior Talent Research Foundation of Jiangsu University (No.23JDG030, 22GDG017), the RGC Postdoctoral Fellowship Scheme of Hong Kong (RGC-PDFS-2324-2S04), and the Postgraduate Research & Practice Innovation Program of Jiangsu Province (KYCX24\_3952, SJCX24\_2419). This work was financially supported by the research project approval of Jiangsu University (23A046, Y23A145).

**Data Availability Statement:** Data are contained within the article.

**Conflicts of Interest:** The authors declare no conflicts of interest.

## References

1. Aresta, M.; Dibenedetto, A.; Angelini, A. Catalysis for the valorization of exhaust carbon: From  $\text{CO}_2$  to chemicals, materials, and fuels. technological use of  $\text{CO}_2$ . *Chem. Rev.* **2014**, *114*, 1709–1742.
2. Yin, S.; Sun, L.; Zhou, Y.; Li, X.; Li, J.; Song, X.; Huo, P.; Wang, H.; Yan, Y. Enhanced electron-hole separation in  $\text{SnS}_2/\text{Au}/\text{g-C}_3\text{N}_4$  embedded structure for efficient  $\text{CO}_2$  photoreduction. *Chem. Eng. J.* **2021**, *406*, 126776. [[CrossRef](#)]
3. Ma, W.; Wang, N.; Guo, Y.; Yang, L.; Lv, M.; Tang, X.; Li, S. Enhanced photoreduction  $\text{CO}_2$  activity on  $\text{g-C}_3\text{N}_4$ : By synergistic effect of nitrogen defective-enriched and porous structure, and mechanism insights. *Chem. Eng. J.* **2020**, *388*, 124288. [[CrossRef](#)]
4. Zhu, Z.; Xing, X.; Qi, Q.; Shen, W.; Wu, H.; Li, D.; Li, B.; Liang, J.; Tang, X.; Zhao, J.; et al. Fabrication of Graphene Modified  $\text{CeO}_2/\text{g-C}_3\text{N}_4$  Heterostructures for Photocatalytic Degradation of Organic Pollutants. *Chin. J. Struct. Chem.* **2023**, *42*, 100194. [[CrossRef](#)]
5. Tang, X.; Shen, W.; Li, D.; Li, B.; Wang, Y.; Song, X.; Zhu, Z.; Huo, P. Research on cobalt-doping sites in  $\text{g-C}_3\text{N}_4$  framework and photocatalytic reduction  $\text{CO}_2$  mechanism insights. *J. Alloys Compd.* **2023**, *954*, 170044. [[CrossRef](#)]
6. Mo, Z.; Miao, Z.; Yan, P.; Sun, P.; Wu, G.; Zhu, X.; Ding, C.; Zhu, Q.; Lei, Y.; Xu, H. Electronic and energy level structural engineering of graphitic carbon nitride nanotubes with B and S co-doping for photocatalytic hydrogen evolution. *J. Colloid Interface Sci.* **2023**, *645*, 525–532. [[CrossRef](#)] [[PubMed](#)]
7. Li, H.; Cheng, C.; Yang, Z.; Wei, J. Encapsulated CdSe/CdS nanorods in double-shelled porous nanocomposites for efficient photocatalytic  $\text{CO}_2$  reduction. *Nat. Commun.* **2022**, *13*, 6466. [[CrossRef](#)]
8. Chang, X.; Wang, T.; Gong, J.  $\text{CO}_2$  Photo-reduction: Insights into  $\text{CO}_2$  Activation and Reaction on Surfaces of Photocatalysts. *Energy Environ. Sci.* **2016**, *9*, 2177–2196.
9. Pathak, P.; Mezziani, M.J.; Li, Y.; Cureton, L.T.; Sun, Y.-P. Improving photoreduction of  $\text{CO}_2$  with homogeneously dispersed nanoscale  $\text{TiO}_2$  catalysts. *Chem. Commun.* **2004**, *10*, 1234–1235. [[CrossRef](#)]
10. Kočí, K.; Obalová, L.; Matějová, L.; Plachá, D.; Lacný, Z.; Jirkovský, J.; Šolcová, O. Effect of  $\text{TiO}_2$  particle size on the photocatalytic reduction of  $\text{CO}_2$ . *Appl. Catal. B Environ.* **2009**, *89*, 494–502. [[CrossRef](#)]
11. Wang, Y.; Li, B.; Zhang, C.; Cui, L.; Kang, S.; Li, X.; Zhou, L. Ordered mesoporous  $\text{CeO}_2\text{-TiO}_2$  composites: Highly efficient photocatalysts for the reduction of  $\text{CO}_2$  with  $\text{H}_2\text{O}$  under simulated solar irradiation. *Appl. Catal. B Environ.* **2013**, *130–131*, 277–284. [[CrossRef](#)]
12. Li, Y.; Wang, W.-N.; Zhan, Z.; Woo, M.-H.; Wu, C.-Y.; Biswas, P. Photocatalytic reduction of  $\text{CO}_2$  with  $\text{H}_2\text{O}$  on mesoporous silica supported  $\text{Cu}/\text{TiO}_2$  catalysts. *Appl. Catal. B Environ.* **2010**, *100*, 386–392. [[CrossRef](#)]

13. Zhu, Z.; Ye, J.; Tang, X.; Chen, Z.; Yang, J.; Huo, P.; Ng, Y.; Crittenden, J. Vacancy-Rich CoSx@LDH@Co-NC Catalytic Membrane for Antibiotic Degradation with Mechanistic Insights. *Environ. Sci. Technol.* **2023**, *57*, 16131–16140. [[CrossRef](#)]
14. Zhao, X.; Xu, M.; Song, X.; Zhou, W.; Liu, X.; Yan, Y.; Huo, P. Charge separation and transfer activated by covalent bond in UiO-66-NH<sub>2</sub>/RGO heterostructure for CO<sub>2</sub> photoreduction. *Chem. Eng. J.* **2022**, *437*, 135210. [[CrossRef](#)]
15. Ye, Q.; Zhou, Y.; Xu, Y.; Zhang, Q.; Shi, X.; Li, D.; Tian, D.; Jiang, D. Improved charge transfer in polymeric carbon nitride synergistically induced by the aromatic rings modification and Schottky junctions for efficient photocatalytic CO<sub>2</sub> reduction. *Chem. Eng. J.* **2023**, *463*, 142395. [[CrossRef](#)]
16. Hammond, O.S.; Edler, K.J.; Bowron, D.T.; Torrente-Murciano, L. Deep eutectic-solvothermal synthesis of nanostructured ceria. *Nat. Commun.* **2017**, *8*, 14150. [[CrossRef](#)]
17. Wang, Z.; Yu, R. Hollow Micro/Nanostructured Ceria-Based Materials: Synthetic Strategies and Versatile Applications. *Adv. Mater.* **2018**, *31*, e1800592. [[CrossRef](#)]
18. Huang, X.; Zhang, K.; Peng, B.; Wang, G.; Muhler, M.; Wang, F. Ceria-Based Materials for Thermocatalytic and Photocatalytic Organic Synthesis. *ACS Catal.* **2021**, *11*, 9618–9678. [[CrossRef](#)]
19. Selopal, G.S.; Zhao, H.; Wang, Z.M.; Rosei, F. Core/Shell Quantum Dots Solar Cells. *Adv. Funct. Mater.* **2020**, *30*, 1908762. [[CrossRef](#)]
20. Ning, Z.; Tian, H.; Yuan, C.; Fu, Y.; Qin, H.; Sun, L.; Ågren, H. Solar cells sensitized with type-II ZnSe–CdS core/shell colloidal quantum dots. *Chem. Commun.* **2011**, *47*, 1536–1538. [[CrossRef](#)] [[PubMed](#)]
21. Kouhnavard, M.; Ikeda, S.; Ludin, N.; Khairudin, N.A.; Ghaffari, B.; Mat-Teridi, M.; Ibrahim, M.; Sepeai, S.; Sopian, K. A review of semiconductor materials as sensitizers for quantum dot-sensitized solar cells. *Renew. Sustain. Energy Rev.* **2014**, *37*, 397–407. [[CrossRef](#)]
22. Yakoubi, A.; Ben Chaabane, T.; Aboulaich, A.; Mahiou, R.; Balan, L.; Medjahdi, G.; Schneider, R. Aqueous synthesis of Cu-doped CdZnS quantum dots with controlled and efficient photoluminescence. *J. Lumin.* **2016**, *175*, 193–202. [[CrossRef](#)]
23. Saha, S.; Sain, S.; Meikap, A.; Pradhan, S. Microstructure characterization and electrical transport of nanocrystalline CdZnS quantum dots. *Phys. E Low-Dimens. Syst. Nanostruct.* **2015**, *66*, 59–66. [[CrossRef](#)]
24. Yang, H.; Xu, B.; Zhang, Q.; Yuan, S.; Zhang, Z.; Liu, Y.; Nan, Z.; Zhang, M.; Ohno, T. Boosting visible-light-driven photocatalytic performance of waxberry-like CeO<sub>2</sub> by samarium doping and silver QDs anchoring. *Appl. Catal. B Environ.* **2021**, *286*, 119845. [[CrossRef](#)]
25. Jiang, H.; Li, X.; Chen, S.; Wang, H.; Huo, P. g-C<sub>3</sub>N<sub>4</sub> quantum dots-modified mesoporous CeO<sub>2</sub> composite photocatalyst for enhanced CO<sub>2</sub> photoreduction. *J. Mater. Sci. Mater. Electron.* **2020**, *31*, 20495–20512. [[CrossRef](#)]
26. Sre, V.V.; Okla, M.K.; Janani, B.; Abdel-Maksoud, M.A.; Al-Amri, S.S.; Alaraidh, I.A.; Alatar, A.A.; Khan, S.S. A novel sunlight driven Z scheme ZnCdS QDs deposited over g-C<sub>3</sub>N<sub>4</sub> photocatalyst for photoinactivation of E. coli cells. *J. Water Process. Eng.* **2024**, *59*, 104957. [[CrossRef](#)]
27. Morgan, D.J. Photoelectron spectroscopy of ceria: Reduction, quantification and the myth of the vacancy peak in XPS analysis. *Surf. Interface Anal.* **2023**, *55*, 845–850. [[CrossRef](#)]
28. Zhang, Y.; Li, J.; Zhou, W.; Liu, X.; Song, X.; Chen, S.; Wang, H.; Huo, P. Rational design of Ag/CuO@ZnIn<sub>2</sub>S<sub>4</sub> S-scheme plasmonic photocatalyst for highly selective CO<sub>2</sub> conversion. *Appl. Catal. B Environ.* **2024**, *342*, 123449.
29. Boaro, M.; Colussi, S.; Trovarelli, A. Ceria-Based Materials in Hydrogenation and Reforming Reactions for CO<sub>2</sub> Valorization. *Front. Chem.* **2019**, *7*, 28. [[CrossRef](#)]
30. Mullins, D.R. The surface chemistry of cerium oxide. *Surf. Sci. Rep.* **2015**, *70*, 42–85. [[CrossRef](#)]
31. Rodriguez, J.A.; Grinter, D.C.; Liu, Z.; Palomino, R.M.; Senanayake, S.D. Ceria-based model catalysts: Fundamental studies on the importance of the metal–ceria interface in CO oxidation, the water–gas shift, CO<sub>2</sub> hydrogenation, and methane and alcohol reforming. *Chem. Soc. Rev.* **2017**, *46*, 1824–1841. [[CrossRef](#)] [[PubMed](#)]
32. Kim, S.S.; Britcher, L.; Kumar, S.; Griesser, H.J. XPS Study of Sulfur and Phosphorus Compounds with Different Oxidation States. *Sains Malays.* **2018**, *47*, 1913–1922. [[CrossRef](#)]
33. Wu, L.; Su, F.; Liu, T.; Liu, G.-Q.; Li, Y.; Ma, T.; Wang, Y.; Zhang, C.; Yang, Y.; Yu, S.-H. Phosphorus-Doped Single-Crystalline Quaternary Sulfide Nanobelts Enable Efficient Visible-Light Photocatalytic Hydrogen Evolution. *J. Am. Chem. Soc.* **2022**, *144*, 20620–20629. [[CrossRef](#)]
34. Sun, Y.; Hao, Y.; Lin, X.; Liu, Z.; Sun, H.; Jia, S.; Chen, Y.; Yan, Y.; Li, X. Efficient electron transport by 1D CuZnInS modified 2D Ti<sub>3</sub>C<sub>2</sub> MXene for enhanced photocatalytic hydrogen production. *J. Colloid Interface Sci.* **2024**, *653*, 396–404. [[CrossRef](#)] [[PubMed](#)]
35. Kim, S.-J.; Choi, M.; Hong, G.; Hahn, S.K. Controlled afterglow luminescent particles for photochemical tissue bonding. *Light Sci. Appl.* **2022**, *11*, 314. [[CrossRef](#)] [[PubMed](#)]
36. Zhao, J.; Wang, Y.; Li, Y.; Yue, X.; Wang, C. Phase-dependent enhancement for CO<sub>2</sub> photocatalytic reduction over CeO<sub>2</sub>/TiO<sub>2</sub> catalysts. *Catal. Sci. Technol.* **2016**, *6*, 7967–7975. [[CrossRef](#)]
37. Kibar, M.E. Preparation of copper oxide-cerium oxide/nanotube-titanium dioxide photocatalyst for CO<sub>2</sub> conversion in solar light. *React. Kinet. Catal. Lett.* **2021**, *134*, 937–950. [[CrossRef](#)]
38. Hu, H.; Hu, J.; Wang, X.; Gan, J.; Su, M.; Ye, W.; Zhang, W.; Mac, X.; Huihu, W. Enhanced reduction and oxidation capability over CeO<sub>2</sub>/g-C<sub>3</sub>N<sub>4</sub> hybrid through surface carboxylation: Performance and mechanism. *Catal. Sci. Technol.* **2020**, *10*, 4712–4725. [[CrossRef](#)]



39. Li, Z.; Liu, Z.; Li, Y.; Wang, Q. Flower-like CoAl layered double hydroxides modified with CeO<sub>2</sub> and RGO as efficient photocatalyst towards CO<sub>2</sub> reduction. *J. Alloys Compd.* **2021**, *881*, 160650. [[CrossRef](#)]
40. Su, B.; Kong, Y.; Wang, S.; Zuo, S.; Lin, W.; Fang, Y.; Hou, Y.; Zhang, G.; Zhang, H.; Wang, X. Hydroxyl-Bonded Ru on Metallic TiN Surface Catalyzing CO<sub>2</sub> Reduction with H<sub>2</sub>O by Infrared Light. *J. Am. Chem. Soc.* **2023**, *145*, 27415–27423. [[CrossRef](#)]
41. Yin, S.; Zhou, Y.; Liu, Z.; Wang, H.; Zhao, X.; Zhu, Z.; Yan, Y.; Huo, P. Elucidating protonation pathways in CO<sub>2</sub> photoreduction using the kinetic isotope effect. *Nat. Commun.* **2024**, *15*, 437. [[CrossRef](#)] [[PubMed](#)]
42. Xu, J.; Ju, Z.; Zhang, W.; Pan, Y.; Zhu, J.; Mao, J.; Zheng, X.; Fu, H.; Yuan, M.; Chen, H.; et al. Efficient Infrared-Light-Driven CO<sub>2</sub> Reduction Over Ultrathin Metallic Ni-doped CoS<sub>2</sub> Nanosheets. *Angew. Chem. Int. Ed.* **2021**, *60*, 8705–8709. [[CrossRef](#)] [[PubMed](#)]
43. Liu, L.; Huang, H.; Chen, Z.; Yu, H.; Wang, K.; Huang, J.; Yu, H.; Zhang, Y. Synergistic Polarization Engineering on Bulk and Surface for Boosting CO<sub>2</sub> Photoreduction. *Angew. Chem. Int. Ed.* **2021**, *60*, 18303–18308. [[CrossRef](#)] [[PubMed](#)]
44. Song, X.; Wu, Y.; Zhang, X.; Li, X.; Zhu, Z.; Ma, C.; Yan, Y.; Huo, P.; Yang, G. Boosting charge carriers separation and migration efficiency via fabricating all organic van der Waals heterojunction for efficient photoreduction of CO<sub>2</sub>. *Chem. Eng. J.* **2021**, *408*, 127292. [[CrossRef](#)]
45. Zhu, K.; Zhu, Q.; Jiang, M.; Zhang, Y.; Shao, Z.; Geng, Z.; Wang, X.; Zeng, H.; Wu, X.; Zhang, W.; et al. Modulating Ti<sub>2g</sub> Orbital Occupancy in a Cu/TiO<sub>2</sub> Composite for Selective Photocatalytic CO<sub>2</sub> Reduction to CO. *Angew. Chem. Int. Ed.* **2022**, *61*, e202207600. [[CrossRef](#)]
46. Chen, Y.; Yu, S.; Fan, X.-B.; Wu, L.-Z.; Zhou, Y. Mechanistic insights into the influence of surface ligands on quantum dots for photocatalysis. *J. Mater. Chem. A* **2023**, *11*, 8497–8514. [[CrossRef](#)]
47. Xiao, Y.; Jiang, Y.; Zhou, E.; Zhang, W.; Liu, Y.; Zhang, J.; Wu, X.; Qi, Q.; Liu, Z. In-suit fabricating an efficient electronic transport channels via S-scheme polyaniline/Cd<sub>0.5</sub>Zn<sub>0.5</sub>S heterojunction for rapid removal of tetracycline hydrochloride and hydrogen production. *J. Mater. Sci. Technol.* **2023**, *153*, 205–218. [[CrossRef](#)]
48. Xu, S.; Jiang, G.; Zhang, H.; Gao, C.; Chen, Z.; Liu, Z.; Wang, J.; Du, J.; Cai, B.; Li, Z. Boosting Photocatalytic CO<sub>2</sub> Methanation through Interface Fusion over CdS Quantum Dot Aerogels. *Small* **2024**, e2400769. [[CrossRef](#)]
49. Zhang, Z.; Rogers, C.R.; Weiss, E.A. Energy Transfer from CdS QDs to a Photogenerated Pd Complex Enhances the Rate and Selectivity of a Pd-Photocatalyzed Heck Reaction. *J. Am. Chem. Soc.* **2019**, *142*, 495–501. [[CrossRef](#)]
50. Aldana, J.; Wang, Y.A.; Peng, X. Photochemical Instability of CdSe Nanocrystals Coated by Hydrophilic Thiols. *J. Am. Chem. Soc.* **2001**, *123*, 8844–8850. [[CrossRef](#)]

**Disclaimer/Publisher's Note:** The statements, opinions and data contained in all publications are solely those of the individual author(s) and contributor(s) and not of MDPI and/or the editor(s). MDPI and/or the editor(s) disclaim responsibility for any injury to people or property resulting from any ideas, methods, instructions or products referred to in the content.